LA-UR -83-2150

CONF-830932--7

D7-0091-4

LA-UR--83-2150

DE83 015221

Los Alamos National Laboratory is operated by the University of California for the United States Department of Energy under contract W-7405-ENG-36

TITLE: VARIATIONAL METHODS IN STEADY STATE DIFFUSION PROBLEMS

AUTHOR(S): Clarence E. Lee

NOTICE

THIS REPORT IS ILLEGIBLE TO A A DEGREE THAT PRECLUDES SATISFACTORY REPRODUCTION

SUBMITTED TO: Canadian Nuclear Society Meeting
Spetember 6, 1983

Los Alamos National Laboratory
Los Alamos, New Mexico 87545

FORM NO 836 R4
ST NO 2629 5/81

DISCLAIMER

VARIATIONAL METHODS IN STEADY STATE DIFFUSION PROBLEMS

Clarence E. Lee[+]
Wesley C.F. Fan
Robert L. Bratton

Department of Nuclear Engineering
Texas A & M University
College Station, Texas, 77843

ABSTRACT

Classical variational techniques are used to obtain accurate solutions to the multigroup multiregion one dimensional steady state neutron diffusion equation. Analytic solutions are constructed for benchmark verification. Functionals with cubic trial functions and conservational lagrangian constraints are exhibited and compared with nonconservational functionals with respect to neutron balance and to relative flux and current at interfaces. Excellent agreement of the conservational functionals using cubic trial functions is obtained in comparison with analytic solutions.

We investigate numerical solutions to the neutron diffusion problem using classical variational techniques and shape functions consistent with continuity conditions. Using the multigroup approximation, we define the flux as $\emptyset(r)$ and the adjoint as $\emptyset^+(r)$, each are vectors of length G, the number of groups. The multigroup flux diffusion equation is given by

$$D\,\emptyset = L\,\emptyset - h\,F\,\emptyset = 0,$$

and the adjoint equation is given by

$$D^+\,\emptyset^+ = L^+\,\emptyset^+ - h^+\,F^+\,\emptyset^+ = 0,$$

where h and h^+ are the eigenvalues, L and L^+ represent the diffusion flux and adjoint operators, including leakage, absorption, and scattering term contributions, and F and F^+ represent the fission and adjoint fission operators, respectively. We form the functional $G[\emptyset^+,\emptyset]$ defined by

$$G[\emptyset^+,\emptyset] = \langle \emptyset^+, D\emptyset \rangle = \langle \emptyset, D^+\emptyset^+ \rangle,$$

where the $\langle , \rangle$ notation implies inner product integration over spatial variables and sums over the groups in the multigroup approximation. We assume that the flux and adjoint functions satisfy the same boundary conditions. Taking the variation of $G[\emptyset^+,\emptyset]$ with respect to $\emptyset$ and $\emptyset^+$ yields the diffusion equations for $\emptyset^+$ and $\emptyset$, respectively. This formulation of $G[\emptyset^+,\emptyset]$ is well-known and straightforward. Quadratic-like forms for one group self-adjoint operators (Galerkin methods) are obtained provided integration by parts of the laplacian

----

[+] Consultant, Applied Theoretical Physics Division, Los Alamos National Laboratory, Los Alamos, New Mexico.

terms exhibit continuity when evaluated at boundaries. Boundary condition constraints can be appended to $G[\phi^+,\phi]$, as discussed by numerous authors.[2]

In developing one dimensional numerical schemes, we define approximate flux and adjoint functions. Requiring spatial continuity of flux (adjoint) and current (adjoint) at material interfaces, four conditions and four equations apply for each region and group. The cubic trial function solution for the nodal flux (adjoint) and current (adjoint) coefficients at region boundaries which satisfies continuity is given in Appendix 1. Each term in the trial function involves a coefficient times a unique hermite polynomial shape function.[3] Satisfying the continuity conditions in the trial functions eliminates making that additional requirement on the functional $G[\phi^+,\phi]$.

Minimizing $G[\phi^+,\phi]$ with respect to the nodal values (flux, adjoint, current, and adjoint current) of these trial functions yields a set of linear coupled equations in the nodal values for each group. Cubic spatial dependence of the diffusion coefficient and cross sections is allowed, although other integrable forms may be used. Evaluating the polynomial integrals the resulting linear algebraic equations can be solved by standard techniques for source or eigenvalue problems. Since $G[\phi^+,\phi]$ is being minimized the nodal solutions satisfy the original differential equation only at the nodal positions. The function errors between nodes can be quite large. Likewise, the conservation law (the spatial integral of the original equations) is satisfied only approximately for any finite number of nodes. These errors decrease with increasing number of nodes, but could preclude competition with classical finite difference methods if field quantities were of main interest instead of eigenvalues. A constructive solution is obtained by appending the functional with conservational lagrangian constraint terms

$$G^1[\phi^+,\phi,c^+,c] = G[\phi^+,\phi] + \langle c^+,D\phi\rangle + \langle c,D^+\phi^+\rangle,$$

in each cell and energy group, with the corresponding additional implied minimization with respect to the langrange multipliers, c and c^+. The detailed form of the conservational functional with the trial functions substituted is given in Appendix 2. The property $h = h^+$, requisite in diffusion and transport solutions, is also easily satisfied. Performing the minimization for the criticality problem with respect to the cubic trial function nodal values results in matrix equations of the form

$$\begin{bmatrix} A & 0 \\ 0 & A^+ \end{bmatrix}\begin{bmatrix} M \\ M^+ \end{bmatrix} = h \begin{bmatrix} F & 0 \\ 0 & F^+ \end{bmatrix}\begin{bmatrix} M \\ M^+ \end{bmatrix},$$

where the vectors M and M^+ are composed of nodal flux, current, and lagrangian multipliers and their adjoints. The matrix elements of A and A^+ are integrals derived from L and L^+ (leakage, removal, and scattering terms), and the matrix elements of F and F^+ arise from integrals of the fission terms. The corresponding Rayleigh-Ritz determination of the eigenvalue h is given by

$$h = (\langle M,AM\rangle + \langle M^+,A^+M^+\rangle)/(\langle M,FM\rangle + \langle M^+,F^+M^+\rangle).$$

With all these solution properties, it is still possible to generate "negative" fluxes for sufficiently coarse nodal spacings. An automatic node generation scheme can be applied to place the nodes so that a cubic trial function will accurately approximate the solution within each group, and yield positive fluxes. However, for this study, we used only equally spaced nodes, a standard practice found in literature comparisons. All of the reported solutions have positive fluxes everywhere inside the uter boundaries.

We test the accuracy of this methodology by direct comparison to precisely evaluated analytical solutions.[4] The analytical solution technique is summarized in Appendix 3. Both the analytical and variational solutions are evaluated in the same computer program. This procedure allows for direct comparison of the solutions between the variation node placement at problem execution time.

Three problems, two thermal and one fast system, are compared with the analytical multiregion results for varying number of nodes in two,[5] three[6], and four[7,8] groups. The detailed spatial and eigenvalue errors between the analytical and numerical solutions for flux and adjoint are summarized below.

The two group two region problem is a simplistic homogeneous U^{235} cylindrical core of 15 cm radius surrounded by an additional 15 cm water reflector. The ratio of U^{235} atoms to molecules of water is 0.002. The cross sections in Table 1 are taken from Lamarsh.[5] The flux and adjoint solutions for 10 nodes ("5+5") are displayed in Fig. 1. The relative percentage error of the variational solution is compared to the analytical solution in Figs. 2 and 3 for the flux and adjoint, respectively.

The three group two region sphere is a 2.596% enriched U^{235}-UO_2 water moderated system with an H_2O/Fuel volume ratio of 1.844. The 26 cm radius core is surrounded by a 26 cm reflector. The cross sections given in Table 1 are taken form Hirata, et. al.[6] The flux and adjoint solutions for 10 nodes are displayed in Fig. 4. The relative percentage error of the variational solution is compared to the analytical solution in Figs. 5-7 for the flux and adjoint.

The four group two region sphere is a mixed oxide fast core composed of U^{233}-Th with a Th blanket. The 70 cm core radius is surrounded by a 50 cm Th blanket. The cross sections are taken from the report of Ohta, et. al.[7] and Kobayashi and Nishihara.[8] The flux and adjoint solutions for 20 nodes (10 + 10) are displayed in Fig. 8. The relative percentage error of the variational solution is compared to the analytical solution in Figs. 9-12.

From the flux and adjoint solutions, the variational method solution exhibits almost negligible differences from the analytical solutions (the analytical solutions are plotted with a dashed line and differences are discernable in Fig. 4). In the relative percentage error graphs we note that the errors between the nodes are typically of the order of 5 to 100 times the values at the nodes. The errors of the continuous solutions immediately adjacent to the material interfaces are typically 10 to 100 times the adjacent node values. These errors decrease with mesh refinement, but even with only 10 nodes, the errors remain below 1%. In the reflector the relative error increases towards the free surface, but is significant only at the 10 node approximation. At the 20 node approximation the errors are below 1% throughout the reflector. Since the flux has decreased by several orders of magnitude near the outside boundary, this error does not contribute significantly to the absolute values near the free surface.

All the results reported graphically were obtained with the conserving functional $G^1[\emptyset^+,\emptyset,c^+,c]$. If, instead, we use the functional $G[\emptyset,\emptyset] = \langle\emptyset,D\emptyset\rangle$ in multigroup approximation, a Galerkin method, numerous known literature results can be reproduced; however, the method is non-conservative, and one does not obtain $h = h^+$, a desirable basic requirement. Similarly, if we use the variational functional $G[\emptyset^+,\emptyset]$, the method is also non-conservative. However, if we use the functional $G^1[\emptyset^+,\emptyset,c^+,c]$, the solutions are conservative, $h = h^+$, and excellent convergence to the analytical eigenvalues, and the flux and adjoint solutions is obtained.

In Table 2 we compare the k-eff (K) for the conservation (C, using $G^1[\emptyset^+,\emptyset,c^+,c]$) and non-conservation (N-C, using $G[\emptyset^+,\emptyset]$) solution to the analytic solution for the three problems using various equal spaced mesh cells in the core and reflector. The relative error between the numerical and analytical solutions of the flux ($D\emptyset/\emptyset$) and current (DJ/J) at the core-reflector interface are also compared.

We observe that the eigenvalues converge rapidly to the exact analytical results as the mesh is refined. Typically, the k-eff convergence is more rapid than that of the fluxes and currents. The conservational constraint improves the current accuracy at the expense of the flux accuracy for coarse mesh calculations. As the mesh is refined the analytical solution result is approached more rapidly in these problems using the conservational constraint.

In Table 3 we compare the percentage error of neutron balance in each energy group as the mesh is refined. Neutron balance is essentially "exact" (to machine significance) using the conservational constraint, but significant balance errors (4-120%) occur for the coarse mesh non-conservational results. The noted behavior of the coarse mesh non-conservation results could possibly lead to incorrect predictions of conversion or breeding ratios unless a new functional were specifically constructed for that purpose, or the conservational constraint were added.

The application of the lagrangian conservation constraint in coarse mesh calculations results in a relative degradation of the nodal flux accuracy with an improved nodal current accuracy plus neutron balance, compared to the non-conservation results. As the mesh is refined, the conservation constraint nodal flux and current solutions exhibit rapid convergence to the analytical solution.

In conclusion, we have examined a conservational variational method and compared it with analytic solutions to simple problems. When used with cubic hermite polynomial trial functions, derived from flux and current continuity, very accurate solutions to the multigroup multiregion neutron diffusion probem are obtained. Neutron conservation is added to the functional using lagrangian constraints. More accurate flux distributions are obtained with this constraint.

Since the group constants can be spatially dependent between nodes instead of only constant within each material region, the total number of cells needed to represent the material properties and the fluxes (approximated by cubics) is considerably reduced.

The major differences between the variational and Galerkin approach is in the usage of the adjoint weighting function instead of the approximate function itself. Although this variational method doubles the total number of equations to be solved, the resulting flux and adjoint solutions are readily applied for perturbation and/or optimization analysis in design. Neutron conservation is a necessary constraint on the neutron diffusion equation. Even though some approximations exhibit this property with fine mesh spacing, if neutron conservation is not satisfied for all mesh spacings, the resultant solutions can exhibit large errors compared to analytic solutions, and preclude the determination of leakage, removal, scattering, and fission contributions to the solution.

REFERENCES

1. P.M. Morse and H. Feshbach, Methods in Theoretical Physics, vol. 1, ch. 3, McGraw-Hill, New York (1963).
2. J.J. Duderstadt and W.R. Martin, Transport Theory, John Wiley and Sons, New York (1979).
3. J.P. Hennart, "Numerical Methods of High Order Accuracy for One-Dimensional Diffusion Equation," Nucl. Sci. and Eng., vol. 50, pp. 185-199 (1973).
4. C.E. Lee, W.C.P. Fan, and J.S. Rottler, "Diffusion and Kinetics Analytic Benchmark Calculations," Trans. Am. Nucl. Soc., vol. 44, pp. 280-281 (1983).
5. J.R. Lamarsh, Nuclear Reactor Theory, Addison-Wesley Publishing Company, Inc. Reading, Massachusetts, p. 335 (1966).
6. Y. Hirata, Y. Endo, S. Matsura, et. al., "TCA Critical Experiments," JAERI-Memo 1122, Japan Atomic Energy Research Institute (1963).
7. M. Ohta, H. Nishihara, and Y. DeGuchi, " The S4 and Few-Group Diffusion Calculations of Fast Reactors," XXV, Memoirs of the Faculty of Engineering, Kyoto University, Part 3, p. 273 (1974).
8. K. Kobayashi and H. Nishihara, "Solution of the Group-Diffusion Equation Using Green's Function," Nucl. Sci. and Eng., vol. 28, pp. 93-104 (1967).
9. S. Nakamura, Computational Methods in Engineering and Science, John Wiley and Sons, New York (1970).

APPENDIX 1
SUMMARY OF TRIAL FUNCTIONS

A self-consistent choice of trial functions depends upon the properties of the diffusion equation and the imposed boundary conditions for the flux (adjoint) and current (adjoint current) at material interfaces.

Making the standard continuity argument at material interfaces, one finds the cubic hermite polynomial shape functions obtained by Hennart.[3]

Let $w_{gi}(r)$ be a piecewise polynomial for group g in mesh cell i defined at r with the continuity properties

$$w_{gi}(r_i^+) = \emptyset_{gi}, \qquad w_{gi}(r_{i+1}^-) = \emptyset_{gi+1},$$

$$-D_{gi}(r_i^+)\, dw_{gi}(r_i^+)/dr = J_{gi}, \qquad -D_{gi}(r_{i+1}^-)\, dw_{gi}(r_{i+1}^-)/dr = J_{gi+1}.$$

Here the superscripts on the coordinate r indicate evaluation to the left(-) or right(+) of the indicated nodal boundary. The adjoint shape functions are constructed similarily using the adjoint flux and current, but with different interpolation coefficients.

Introducing the dimensionless variable p, in terms of the cell width l_i,

$$p = (r-r_i)/l_i, \quad l_i = r_{i+1} - r_i,$$

we use the above four continuity conditions to solve the assumed cubic trial function form,

$$w_{gi}(p) = a + bp + cp^2 + dp^3,$$

for the coefficients a,b,c, and d. The resulting trial function w_{gi} on the interval [0,1] takes the form

$$w_{gi}(p) = \emptyset_{gi} P_2(p) + \emptyset_{gi+1} P_1(p) - l_i J_{gi} P_4(p)/D_{gi}(r_i^-) + l_i J_{gi+1} P_3(p)/D_{gi}(r_{i+1}^-).$$

The hermite polynomial shape functions, $P_n(p)$, $1 = n = 4$, are given by

$$P_1(p) = (1 + 2p)\,(1-p)^2, \quad P_2(p) = (3 - 2p)\, p^2,$$

$$P_3(p) = (1 - p)\, p^2, \qquad P_4(p) = p\,(1-p)^2,$$

and satisfy the cardinality relations.[3]

Thus, the particular shape functions are derived directly from the continuity conditions. Using the shape function properties the continuity conditions are exactly satisfied on the i^{th} boundary,

$$w_{gi-1}(1) = w_{gi}(0), \qquad D_{gi-1}(r_i^-)\, dw_{gi-1}(1)/dp = D_{gi}(r_i^+)\, dw_{gi}(0)/dp.$$

APPENDIX 2
STRUCTURE OF THE FUNCTIONAL $G^1[\emptyset^+,\emptyset,c^+,c]$

The matrix equations to be solved for the criticality problem can be easily derived from the variational formulation. We use the conservational functional

$$G^1[\emptyset^+,\emptyset,c^+,c] = G[\emptyset^+,\emptyset] + \langle c^+,D\emptyset\rangle + \langle c,D^+\emptyset^+\rangle$$

and substitute the trial functions $w_{gi}(r)$ and $w^+_{gi}(r)$ for the flux and adjoint, respectively. Integrating the leakage terms by parts, we obtain the functional

$$I = G^{1}[w^{+}, w, c^{+}, c]$$

$$= \Sigma^{G}_{g=1} \Sigma^{N}_{i=1} \{(1/l_i) \; {}_0\int^1 D_{gi}(p)\,(dw^{+}_{gi}(p)/dp)\,(dw_{gi}(p)/dp)\,(l_i p + r_i)^a\, dp$$

$$+ l_i \; {}_0\int^1 \Sigma_{Rgi}(p)\, w^{+}_{gi}(p)\, w_{gi}(p)\, (l_i p + r_i)^a\, dp$$

$$- l_i \; \Sigma^{G}_{g'=1, g'\neq g} \; {}_0\int^1 \Sigma_{sg'gi}(p)\, w^{+}_{gi}(p)\, w_{g'i}(p)\, (l_i p + l_i)^a\, dp$$

$$- l_i \; X_{gi}/k \; \Sigma^{G}_{g'=1} \; {}_0\int^1 (v\Sigma_f(p))_{g'i}\, w^{+}_{gi}\, w_{g'i}(p)\, (l_i p + r_i)^a\, dp\}$$

$$+ \; \Sigma^{G}_{g=1} \; \Sigma^{N}_{I=1} \; c^{+}_{gi} \{[r^a_i \; J_{gi} - r^a_{gi+1} \; J_{gi+1}] + l_i \; {}_0\int^1 \Sigma_{Rgi}(p)\, w_{gi}(p)\, ((l_i p + r_i)^a\, dp$$

$$- l_i \; \Sigma^{G}_{g'=1, g'\neq g} \; {}_0\int^1 \Sigma_{sg'gi}(p)\, w_{g'i}(p)\, (l_i p + r_i)^a\, dp$$

$$- l_i \; X_{gi}/k \; \Sigma^{G}_{g'=1} \; {}_0\int^1 (v\Sigma_f(p))_{g'i}\, w_{g'i}(p)\, (l_i p + r_i)^a\, dp\}$$

$$+ \; \Sigma^{G}_{g=1} \; \Sigma^{N}_{i=1} \; c_{gi} \{[r^a_i \; J^{+}_{gi} - r^a_{i+1} \; J^{+}_{gi+1}] + l_i \; {}_0\int^1 \Sigma_{Rgi}(p)\, w^{+}_{gi}(p)\, (l_i p + r_i)^a\, dp$$

$$- l_i \; \Sigma^{G}_{g'=1, g'\neq g} \; {}_0\int^1 \Sigma_{sg'gi}(p)\, w^{+}_{g'i}(p)\, (l_i p + r_i)^a\, dp$$

$$- l_i \; \Sigma^{G}_{g'=1} \; {}_0\int^1 (v\Sigma_f(p))_{gi}\, X_{g'i}\, w^{+}_{g'i}(p)\, (l_i p + r_i)^a\, dp\},$$

where a = 0, 1, and 2 for slab, cylindrical, and spherical geometry, respectively. We have imposed the condition $k = k^{+}$ ($h = 1/k$) at this stage. The non-conservational forms and/or Galerkin forms can be obtained by setting

$$c_{gi} = c^{+}_{gi} = 0, \text{ and/or } w^{+} = w.$$

The functional has undetermined coefficients

$$B_{gi},\; B^{+}_{gi},\; J_{gi},\; J^{+}_{gi},\; c_{gi} \text{ and } c^{+}_{gi}.$$

The shape functions $P_n(p)$, diffusion coefficients, $D_{gi}(p)$, cross sections,

$$\Sigma_{Rgi}(p),\; \Sigma_{sg'gi}(p),\; v\Sigma_f(p)_{gi},$$

and fission spectrum, X_{gi}, are assumed known.

Minimization of the functional with respect to the nodal values of the unknown coefficients requires that

$$\partial I/\partial B_{gi} = \partial I/\partial J_{gi} = \partial I/\partial c^{+}_{gi} = 0,$$

and

$$\partial I/\partial D^{+}_{gi} = \partial I/\partial J^{+}_{gi} = \partial I/\partial c_{gi} = 0,$$

for $g = 1,2,...,G$ and $i = 1,2,...,N+1$, where N = the number of mesh cells. Taking these derivatives and rearranging the equations, the following matrix form is obtained:

$$\begin{bmatrix} B & 0 \\ 0 & B^{+} \end{bmatrix} \begin{bmatrix} M \\ M^{+} \end{bmatrix} = \begin{bmatrix} S & 0 \\ 0 & S^{+} \end{bmatrix} \begin{bmatrix} M \\ M^{+} \end{bmatrix} + h \begin{bmatrix} F & 0 \\ 0 & F^{+} \end{bmatrix} \begin{bmatrix} M \\ M^{+} \end{bmatrix}$$

where B, B^{+}, S, S^{+}, F, and F^{+} are each tridiagonal block matrices containing $3NG \times 3NG$ submatrices, each 3×3. The unknown vectors M and M^{+} of length $3G(N+1)$ are defined as follows:

$$M = [Y_{g1}, Y_{g2}, ..., Y_{gN}, Y_{gN+1}]^{T},$$

and

$$M^{+} = [Y^{+}_{g1}, Y^{+}_{g2}, ..., Y^{+}_{gN}, Y^{+}_{gN+1}]^{T}.$$

Each of the vectors in M and M^{+} are defined by

$$Y_{gi} = [D_{gi}, J_{gi}, c_{gi}]^{T},$$

and

$$Y^{+}_{gi} = [D^{+}_{gi}, J^{+}_{gi}, c^{+}_{gi}]^{T},$$

and contain the unknown nodal coefficients for the flux, current, lagrange multiplier, and the corresponding adjoints. Each of the matrix elements in the matrices B, B^{+}, S, S^{+}, F, and F^{+} are of the integral form given by

$$U_{k,n,m} = {}_{0}\int^{1} u(p)\, d^{k}P_{n}(p)/dp^{k}\, d^{k}P_{m}(p)/dp^{k}\, dp$$

where $k = 0,1$, and $1 \leq n,m \leq 5$, with $P_{5}(p) = 1$, and

$$u(p) = [D_{gi}(p), E_{Rgi}(p), E_{sg'gi}(p), (vE_{f}(p))_{gi}]^{T} (l_{i}p+r_{i})^{a},$$

The matrix elements are evaluated analytically using a recursion relationship derived from the assumed cubic behavior of the flux, diffusion coefficients, and cross sections. This formulation allows taking into account the possible spatial dependence of material properties between nodes.

Defining the matrices $A = B - S$, and $A^{+} = B^{+} - S^{+}$, we have the matrix system

$$\begin{bmatrix} A & 0 \\ 0 & A^{+} \end{bmatrix} \begin{bmatrix} M \\ M^{+} \end{bmatrix} = h \begin{bmatrix} F & 0 \\ 0 & F^{+} \end{bmatrix} \begin{bmatrix} M \\ M^{+} \end{bmatrix}$$

given in the main text. The matrices A, A^{+}, F, and F^{+} are block diagonal. These equations are of the form

$$QX = h\, RX,$$

where Q, X, and R are defined by the previous equation. This matrix eigenvalue problem can be solved iteratively using the Power method, or, after obtaining an estimate, h_{e}, by Wielandt's method in the form

$$(D - h_e R)X = h' RX,$$

where $h = h_e + h'$. In either instance, X is found iteratively after direct inversion of G (Power method) or $(D-h_e R)$ (Wielandt's method). As the problem size increases, eventually computer memory storage requirements will necessitate solving the equations iteratively for each group and using Chebsyschev acceleration of the power iterations.[7]

APPENDIX 3
ANALYTICAL MULTIGROUP MULTIREGION SOLUTIONS

The steady state multigroup diffusion equation for one dimensional problems can be written as

$$\nabla \cdot D_g \nabla \emptyset_g + \Sigma_g \emptyset_g = \Sigma^G_{g'=1} [\Sigma_{sg'g} + (1/k) \Sigma_{fg'g}] \emptyset_{g'} \quad ,$$

where

D_g = Diffusion coefficient in group g,

Σ_g = Total cross section in group g,

$\Sigma_{sg'g}$ = Group transfer cross section from group g' to group g,

$\Sigma_{fg'g}$ = $X_g \, v\Sigma_{fg'}$,

Σ_{fg} = Fission cross section in group g,

X_g = Fission spectrum in group g,

v_g = Average number of neutrons per fission in group g,

and

k = Effective multiplication factor.

The analytical solution to the multigroup diffusion equation is not easily obtained except for simple problems, as, for example, in which the group constants are assumed constant within each spatial region. In this case, for N regions, the diffusion equation takes the form

$$\nabla \cdot D_g \nabla \emptyset_{gn} + \Sigma_g \emptyset_{gn} = \Sigma^G_{g'=1} [\Sigma_{sg'gn} + (1/k) \Sigma_{fg'gn}] \emptyset_{g'n} \quad ,$$

for $n = 1,2,\ldots,N$. For such simplified problems the domain of interest can be divided into N regions with N+1 boundaries. The innermost coordinate is r_1, and the outside boundary is r_{N+1}. The IGN boundary conditions are

$d\emptyset_{g1}(r_1)/dr = 0$ (Symmetry),

$\emptyset_{gN}(r_{N+1}) = 0$ (Zero flux),

$\emptyset_{gn-1}(r_n) = \emptyset_{gn}(r_n)$ (Flux continuity),

and

$D_{gn-1} \, d\emptyset_{gn-1}(r_n)/dr = D_{gn} \, d\emptyset_{gn}(r_n)/dr$ (Current continuity).

The diffusion equation can be rewritten for each region as

$$\nabla^2 \emptyset_{gn} + \Sigma^G_{g'=1} \; S_{ngg'} \, \emptyset_{g'n} = 0,$$

where

$$S_{ngg'} = (\Sigma_{g'n}\,\delta_{g'g} + \Sigma_{sg'g} + (1/k)\Sigma_{fg'g})/D_{gn}.$$

where $\delta_{g'g}$ is the Kronecker delta. Assuming a solution of the form

$$\phi_{gn}(r) = A_{gn}\,Y(w_n r),$$

where the function Y satisfies the Helmholtz equation,

$$\nabla^2 Y - w_n^2\, Y = 0,$$

we have the eigenvalue condition

$$\Sigma^G_{g'=1} (w_n^2\,\delta_{g'g} + S_{ngg'})\,A_{g'n} = 0$$

for g = 1,2,..., G, and n = 1,2,..., N. This result can be written in matrix form as

$$S_n A_n = -w_n^2 A_n$$

where the subscript n indicates the region number, and the dimension of S_n is GxG. The eigenvalues are readily determined by performing a similarity transformation of S_n to upper Hessenberg form, by applying the QR algorithm to solve for the eigenvalues and eigenvectors of the real Hessenberg matrix, and, finally, by applying a similarity transformation to obtain the eigenvectors of the original matrix S_n. In each material region there are G eigenvalues, $-w_{ng}$, and eigenvectors, A_{ng}, which represent coupling coefficients.

The group flux in each region can be expressed as

$$\phi_{gn}(r) = \Sigma^G_{m=1} A_{nmg}\,[p_{nm}\,Y(w_{nm} r) + q_{nm}\,Z(w_{nm} r)]$$

for g = 1,2,...,G and n = 1,2,...,N. The 2GN coefficients, p_{nm} and q_{nm}, can be determined by employing the 2GN boundary conditions. The functions Y(wr) and Z(wr) satisfy the Helmholtz equation for each w. If we let a = 0, 1, and 2 for (infinite symmetric) slab, (infinite symmetric) cylinder, and (symmetric) sphere, the functions Y and Z are given in Table A3.1

TABLE A3.1
HELMHOLTZ SOLUTIONS

a	Y(wr)	Z(wr)
0	cosh(wr)	sinh(wr)
1*	I_0(wr)	K_0(wr)
2	cosh(wr)/r	sinh(wr)/r

* I_0 and K_0 are the modified Bessel functions of the first and second kind.

Using symmetry arguments and the function identification given in Table A3.1 the coefficient q_{1m}, m=1,2,...,G, can be set to zero. Applying the outside boundary condition and the continuity of flux and current at each material interface, we find the matrix equation

$$T\,X = 0,$$

where the vector X contains all the 2G(N-1) unknown p_{nm} and q_{nm}, and the matrix T contains all the coefficients resulting from applying the boundary conditions. The necessary condition for the solution of this homogeneous equation is that the determinant of the matrix T vanish, i.e.

$$\det(T) = 0,$$

which is the criticality condition. A variety of parametric representations for the determination of the critical eigenvalue can be used. For example, k-eff, critical radius for a specified composition, critical composi tion for a specified radius, thickness of one or more regions, etc. In the simplest case, given the critical dimension, a search is performed k to make $\det(T)=0$, or, given the k, a search is performed for the dimension $(r_1,\dots,r_{N+1})$ to make $\det(T)=0$. In this instance, it is assumed that all the group constants are specified. Once the criticality condition is satisfied, a single additional overall normalization ($\phi_g(r) = 1$ at some point for some group or total power) allows the complete numerical evaluation of the group fluxes in each region to be made.

TABLE 1
CROSS SECTIONS

REGION	GROUP	D(cm)	Σ_R	$\nu\Sigma_f\,(cm^{-1})$	χ_g	$\Sigma_{g'g}\,(cm^{-1})$ g'=1	g'=2	g'=3	g'=4
					TWO GROUP TWO REGION CYLINDER				
CORE	1	1.13	0.0419	0.0	1.0	0.0	0.0		
	2	0.16	0.06	0.0845	0.0	0.0419	0.0		
REFLECTOR	1	1.13	0.0419	0.0	0.0	0.0	0.0		
	2	0.16	0.0197	0.0	0.0	0.0419	0.0		
					THREE GROUP TWO REGION SPHERE				
CORE	1	1.475	0.05329	0.869E-3	1.0	0.0	0.0	0.0	
	2	0.709	0.109	1.4908E-2	0.0	5.006E-2	0.0	0.0	
	3	0.233	0.10236	0.16901	0.0	0.0	8.504E-2	0.0	
REFLECTOR	1	1.698	7.372E-2	0.0	0.0	0.0	0.0	0.0	
	2	0.589	0.15262	0.0	0.0	7.252E-2	0.0	0.0	
	3	0.146	1.916E-2	0.0	0.0	0.0	0.15166	0.0	
					FOUR GROUP TWO REGION SPHERE				
CORE	1	3.351	0.3654	9.94141E-3	0.577	0.0	0.0	0.0	0.0
	2	2.456	1.157E-2	8.41634E-3	0.362	2.963E-2	0.0	0.0	0.0
	3	1.870	9.2E-3	9.60889E-3	0.061	2.9E-3	6.7E-3	0.0	0.0
	4	1.259	1.1021E-2	1.46382E-3	0.0	0.0	3.0E-4	3.2E-3	0.0
REFLECTOR	1	2.668	5.531E-2	4.83123E-3	0.577	0.0	0.0	0.0	0.0
	2	2.032	1.051E-2	0.0	0.362	4.736E-2	0.0	0.0	0.0
	3	1.402	8.83E-2	0.0	0.061	5.12E-3	7.3E-3	0.0	0.0
	4	0.976	9.11E-3	0.0	0.0	0.0	4.0E-5	0.0	0.0

TABLE 2

TWO GROUP, TWO REGION CYLINDER
ANALYTIC K = 1.0019437
relative error of thermal flux and current at core-reflector interface

NUMBER OF MESH CELLS	K C	K N-C	DØ/Ø C	DØ/Ø N-C	DJ/J C	DJ/J N-C
2 + 2	1.0023148	1.0021535	3.9E-3	3.5E-3	2.3E-2	2.8E-2
5 + 5	1.0019490	1.0019464	1.1E-5	2.4E-5	1.5E-3	4.1E-3
10 + 10	1.0019438	1.0019438	5.3E-6	1.1E-5	1.1E-4	7.2E-4
15 + 15	1.0019437	1.0019437	2.7E-6	5.3E-6	2.3E-6	2.5E-4
20 + 20	1.0019437	1.0019437	0.0	2.7E-6	7.7E-6	1.1E-4

THREE GROUP, TWO REGION SPHERE
ANALYTIC K = 0.999879
relative error of thermal flux and current at core-reflector interface

NUMBER OF MESH CELLS	K C	K N-C	DØ/Ø C	DØ/Ø N-C	DJ/J C	DJ/J N-C
2 + 2	1.0034584	1.0029754	4.2E-2	2.1E-2	4.0E-1	4.8E-1
5 + 5	1.0000816	1.0000371	7.1E-4	5.4E-4	5.3E-2	1.0E-1
10 + 10	0.9999904	0.9999894	1.3E-4	3.3E-4	5.2E-3	2.2E-2
15 + 15	0.9999882	0.9999881	2.9E-5	9.9E-5	1.1E-3	7.8E-3
20 + 20	0.9999880	0.9999880	6.7E-7	3.0E-5	3.1E-4	3.7E-3

FOUR GROUP, TWO REGION SPHERE
ANALYTIC K = 0.9950425
relative error of first group flux and current at core-blanket interface

NUMBER OF MESH CELLS	K C	K N-C	DØ/Ø C	DØ/Ø N-C	DJ/J C	DJ/J N-C
5 + 5	0.9950465	0.9950428	1.4E-3	1.5E-3	2.9E-3	1.3E-2
10 + 10	0.9950427	0.9950425	1.0E-4	1.4E-4	2.1E-4	2.3E-3
15 + 15	0.9950425	0.9950425	2.0E-5	3.0E-5	4.4E-5	7.7E-4
20 + 20	0.9950425	0.9950425	6.6E-6	1.1E-5	1.4E-5	3.5E-4

TABLE 3

COMPARISON OF NET NEUTRON BALANCE (% ERROR)

NUMBER OF MESH CELLS	GROUP	FOUR GROUP SPHERE C	FOUR GROUP SPHERE N-C	THREE GROUP SPHERE C	THREE GROUP SPHERE N-C	TWO GROUP CYLINDER C	TWO GROUP CYLINDER N-C
2 + 2	1	---	---	-1.11E-13	8.12E+0	1.82E-13	5.44E+1
	2	---	---	1.83E-13	3.58E-1	-6.80E-14	-7.19E-1
	3	---	---	-2.41E-13	4.21E+0		
	4	---	---				
5 + 5	1	-7.03E-11	1.29E+3	3.82E-13	-3.70E-1	4.44E-13	8.56E-1
	2	3.51E-13	1.97E+1	-1.80E-13	1.34E-1	-7.42E-13	3.48E-2
	3	-4.67E-12	1.11E+0	1.44E-13	4.14E+0		
	4	1.81E-12	3.15E-1				
10 + 10	1	3.22E-11	-2.49E+1	2.18E-12	7.89E-1	1.76E-12	3.68E-1
	2	7.13E-11	7.83E+0	2.48E-13	8.60E-2	1.05E-12	8.86E-2
	3	9.27E-13	4.10E-1	-3.87E-14	1.02E+0		
	4	-2.42E-12	1.22E-1				
15 + 15	1	1.07E-10	-2.77E+0	7.27E-12	6.09E-1	1.38E-11	2.25E-1
	2	1.64E-10	5.26E+0	1.20E-12	7.32E-2	6.57E-12	4.90E-2
	3	5.96E-12	2.56E-1	-2.66E-13	5.33E-1		
	4	-7.13E-11	7.68E-2				
20 + 20	1	2.10E-10	9.19E-1	1.19E-11	4.47E-1	2.09E-11	1.59E-1
	2	3.26E-10	3.99E+0	1.97E-12	5.82E-2	1.26E-11	3.44E-2
	3	1.57E-10	1.88E-1	2.64E-12	3.43E-1		
	4	-3.03E-12	5.65E-2				

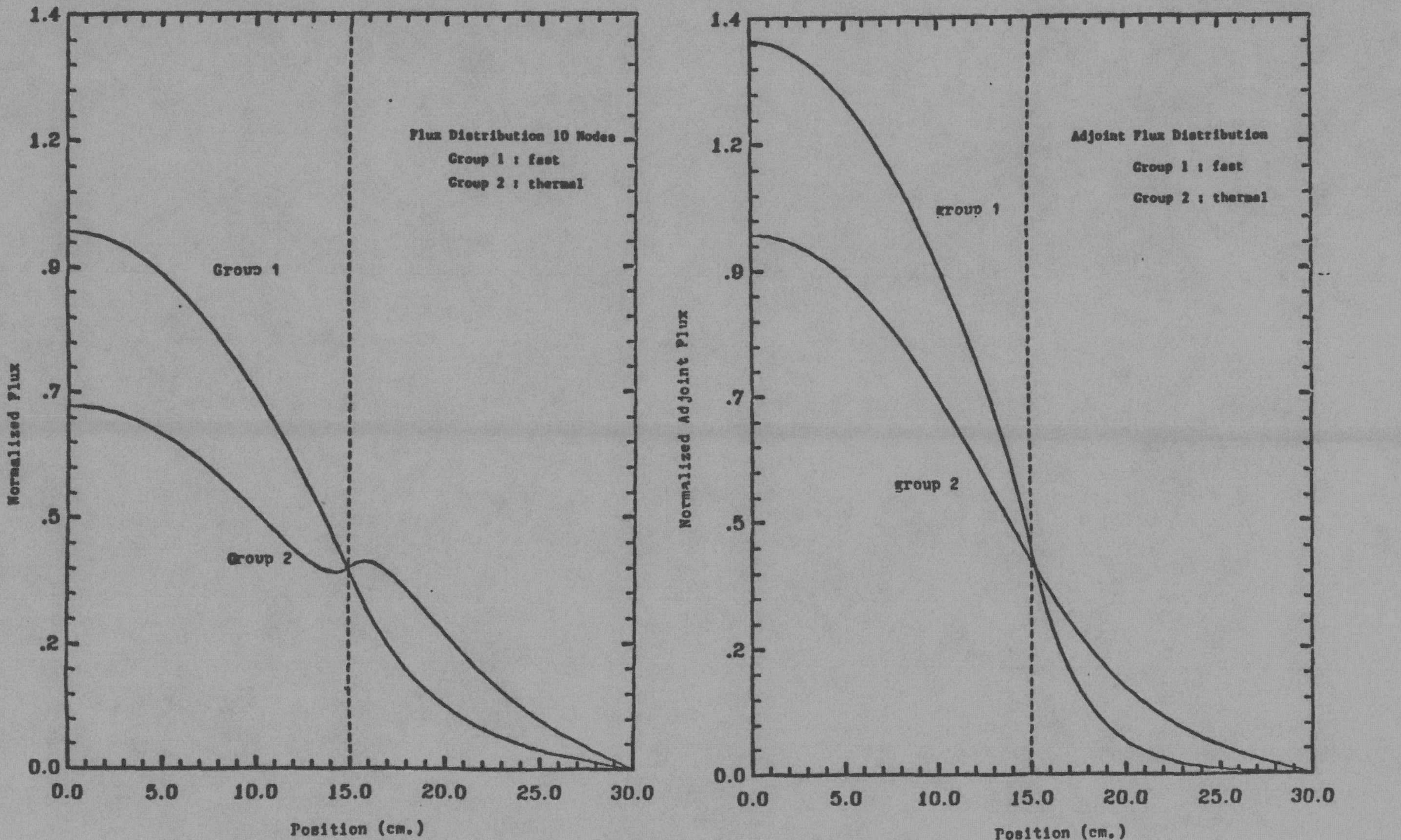

Fig. 1 Flux and Adjoint Distribution

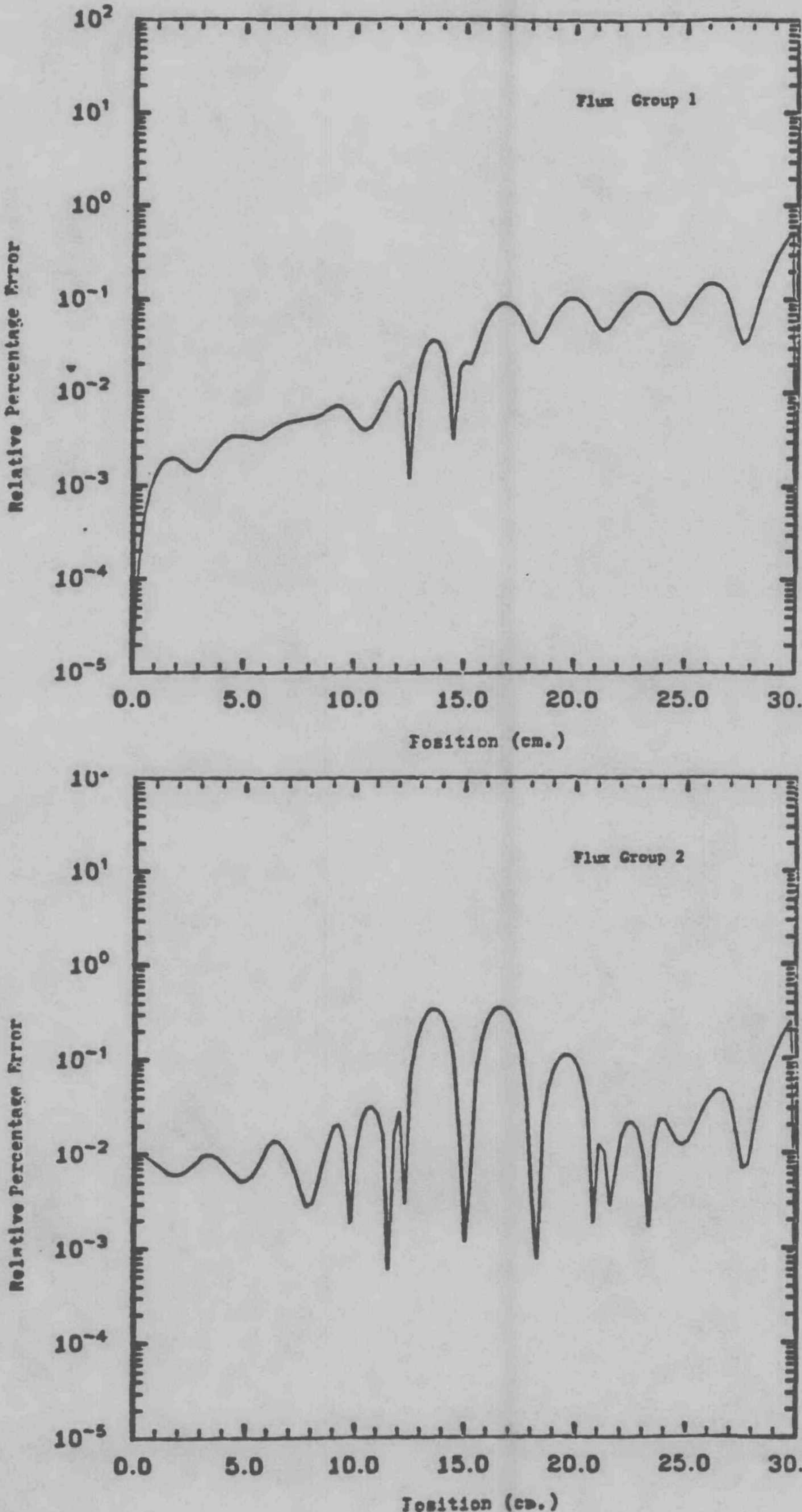

Fig 2 Relative Percentage Error

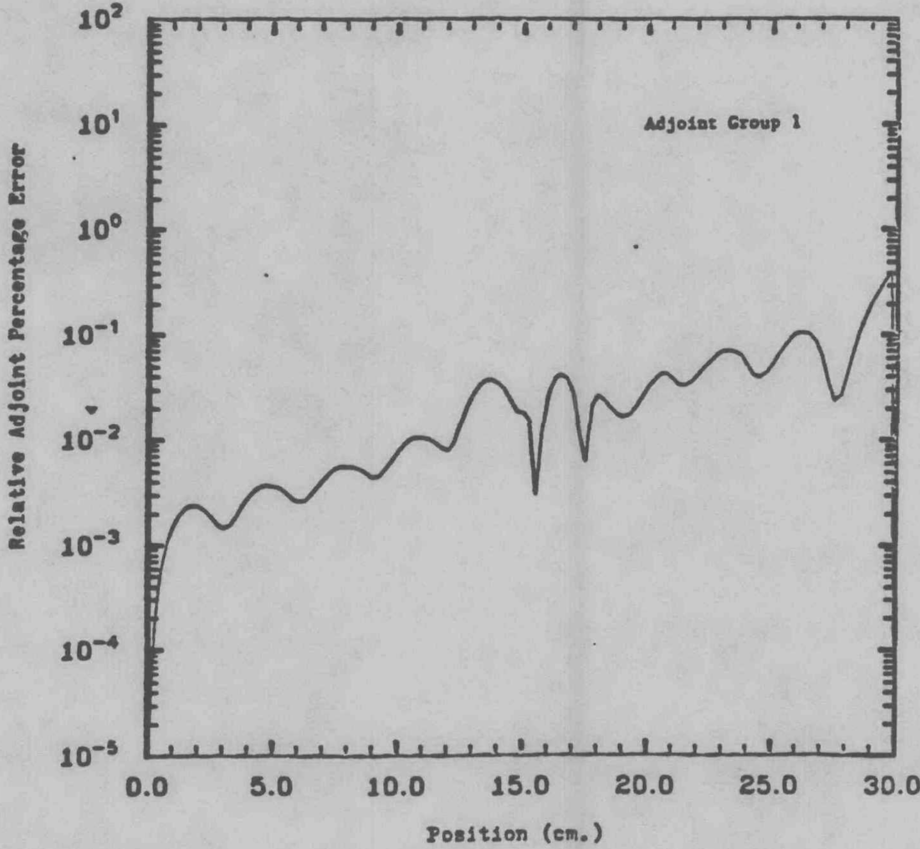

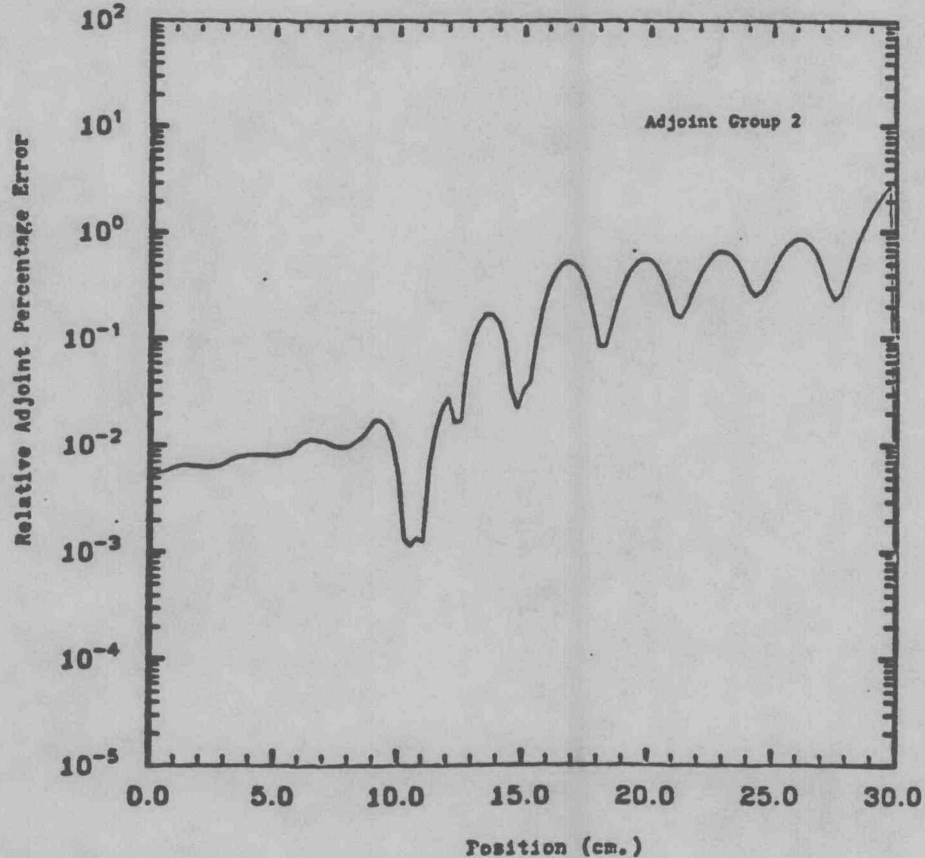

Fig 3 Relative Percentage Error

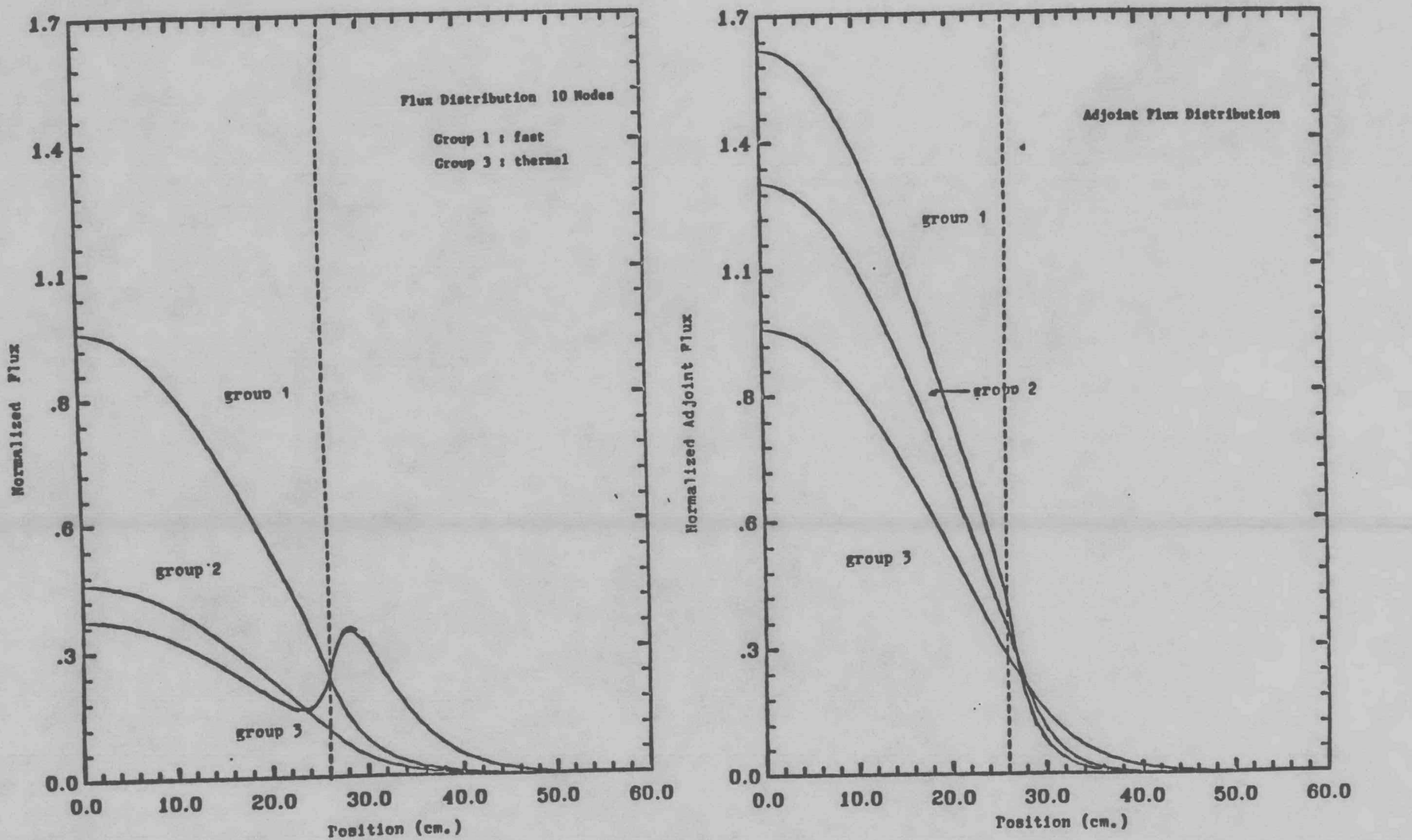

Fig 4 Flux and Adjoint Distribution

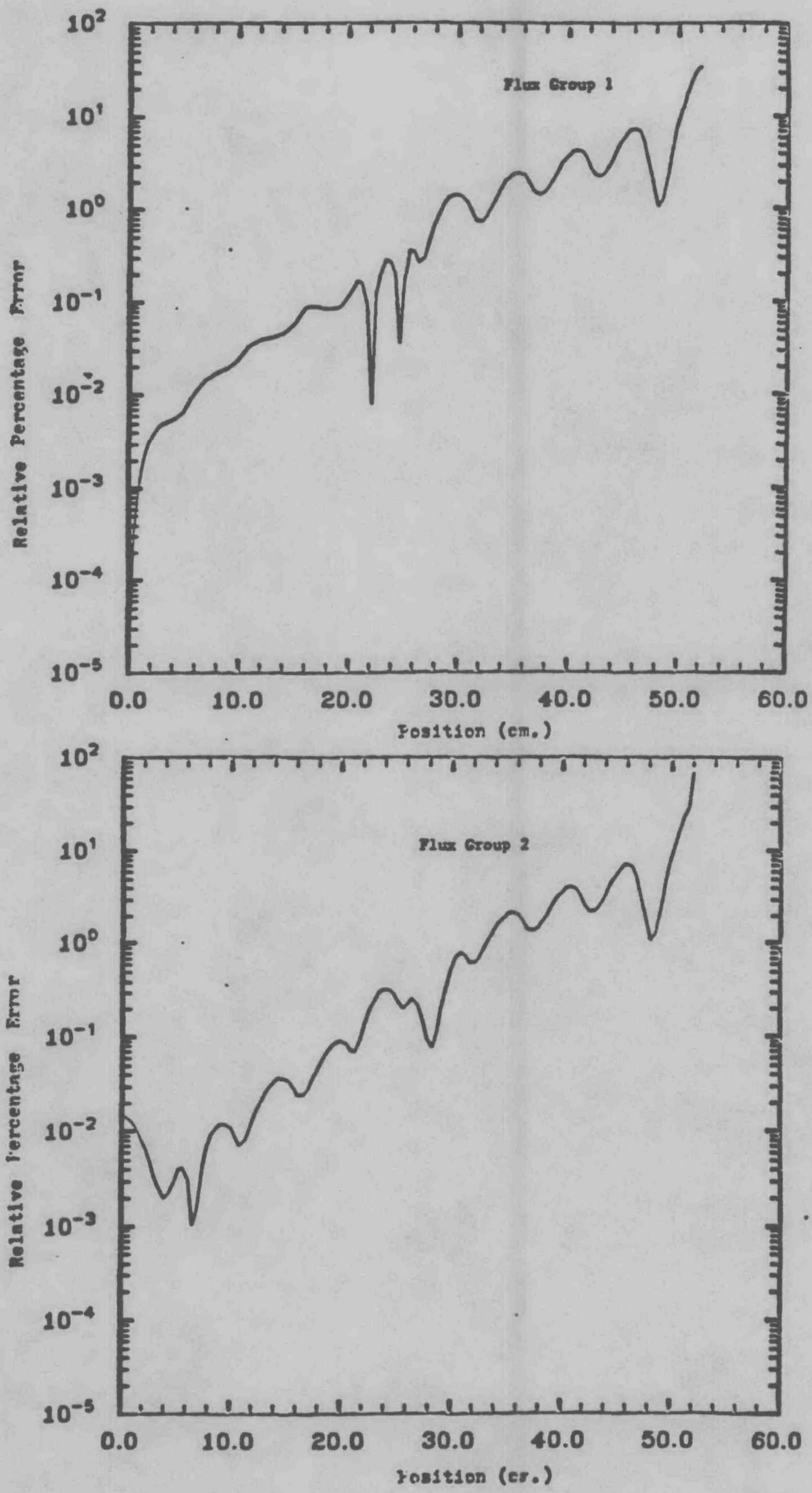

Fig. 5 Relative Percentage Error

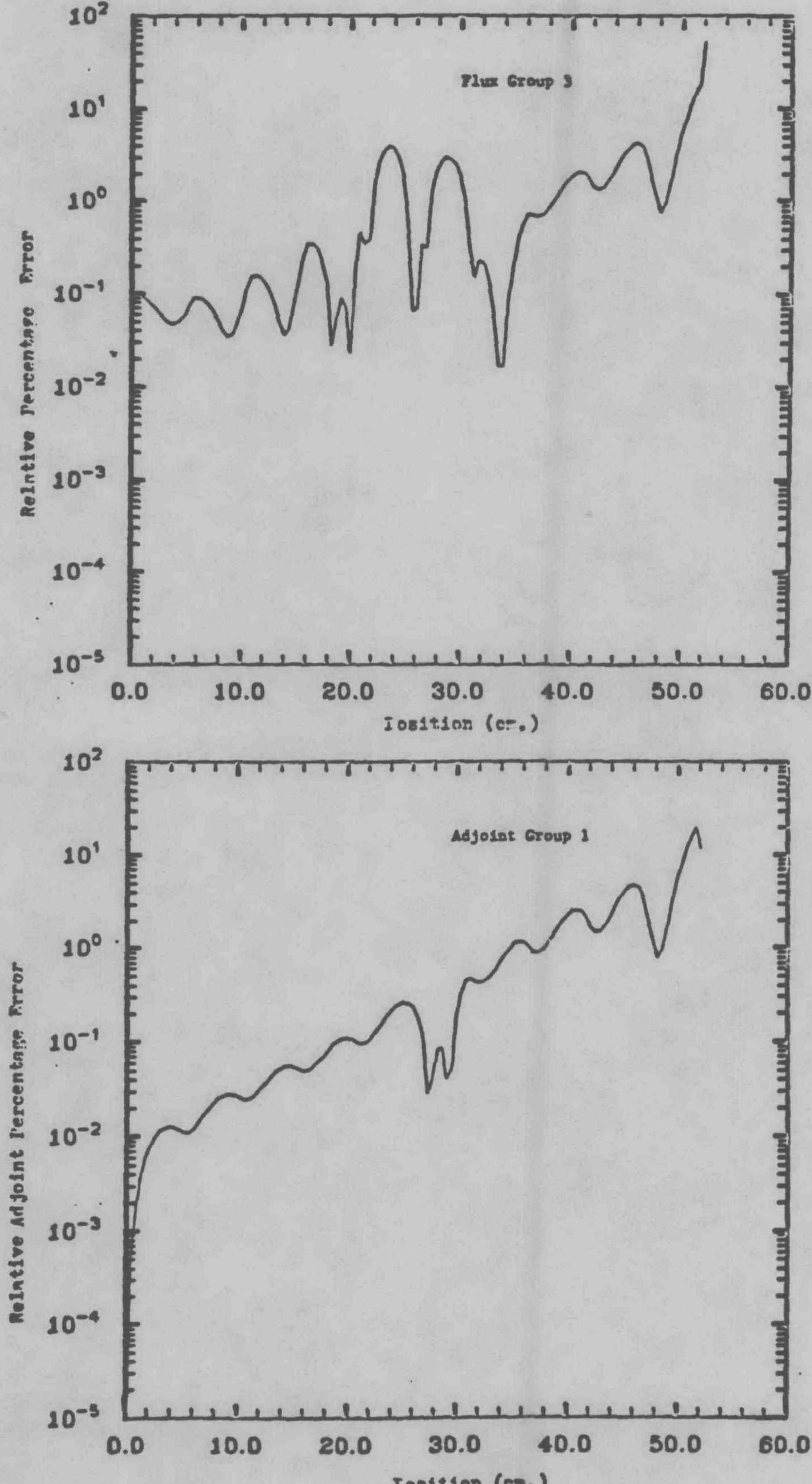

Fig. 6 Relative Percentage Error

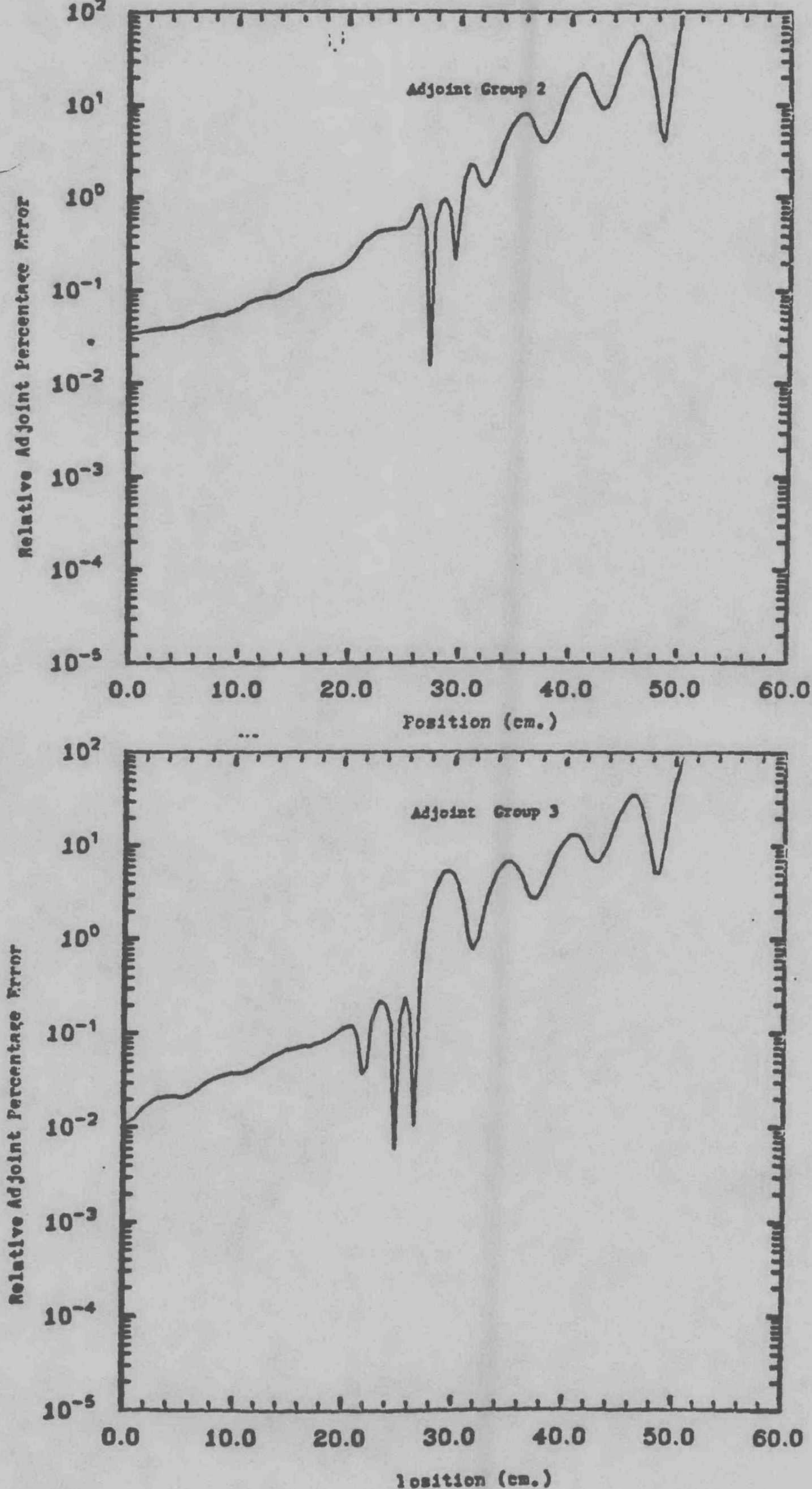

Fig. 7 Relative Percentage Error

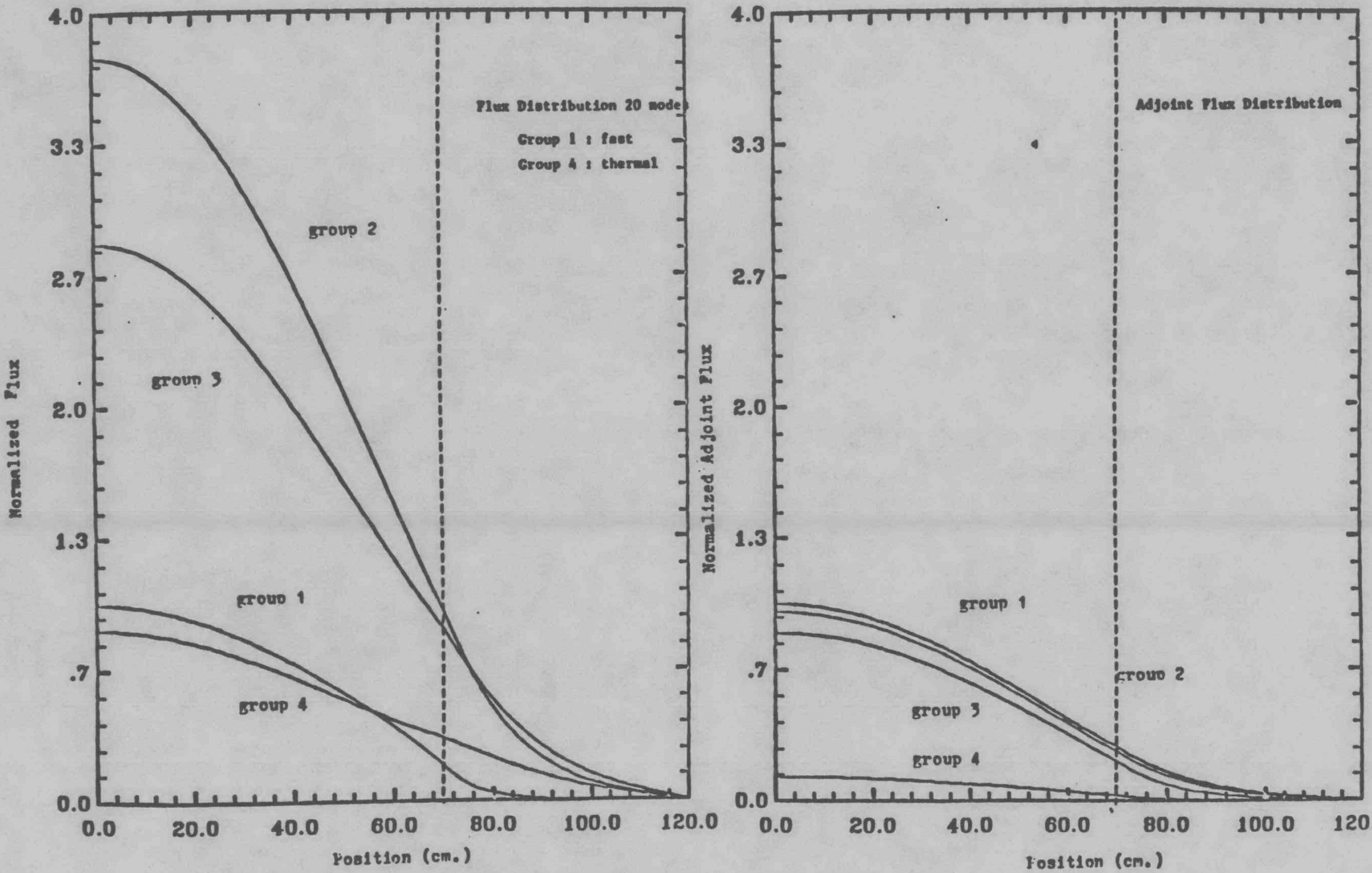

Fig. 8 Flux and Adjoint Distribution

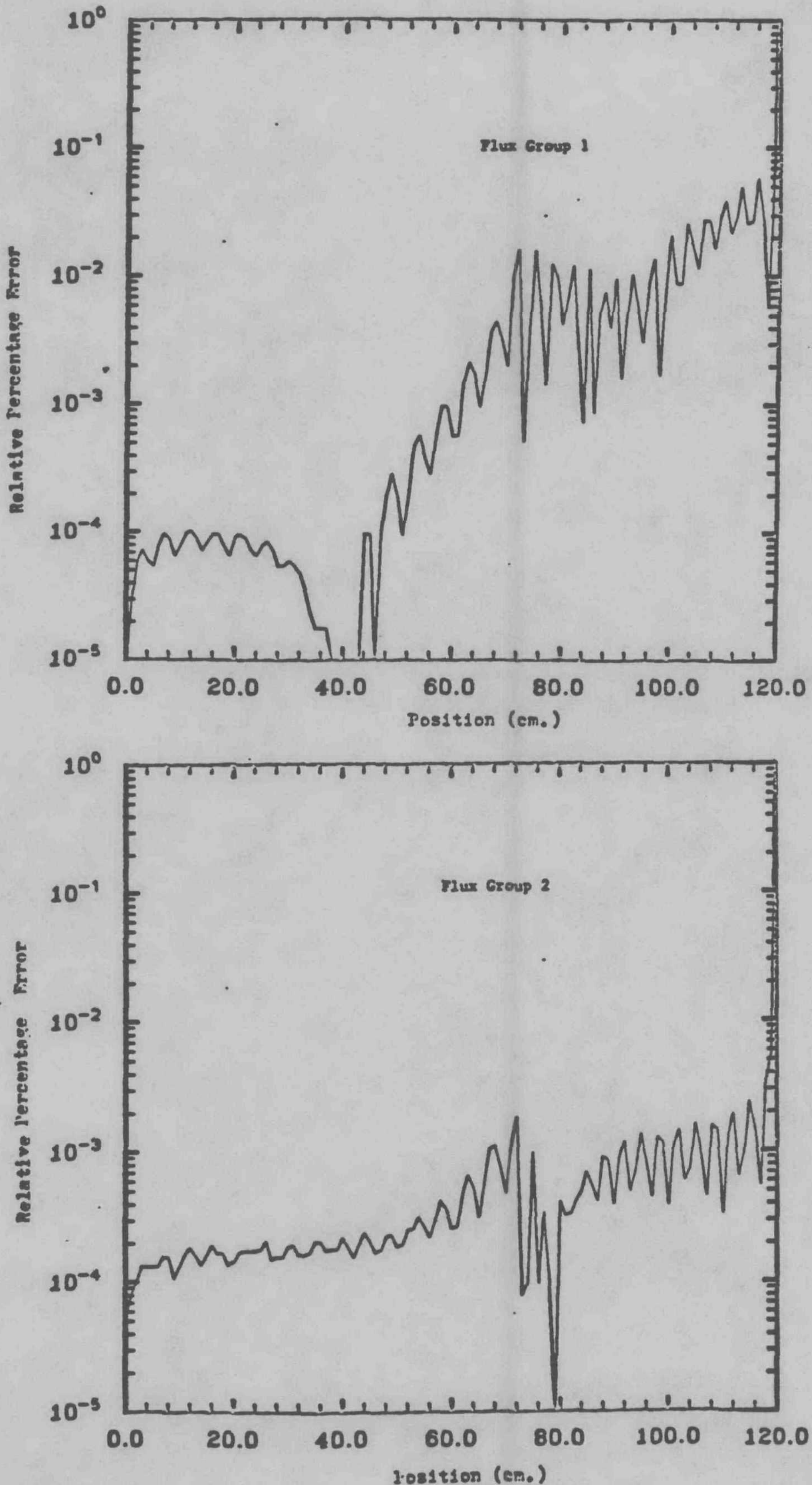

Fig. 9 Relative Percentage Error

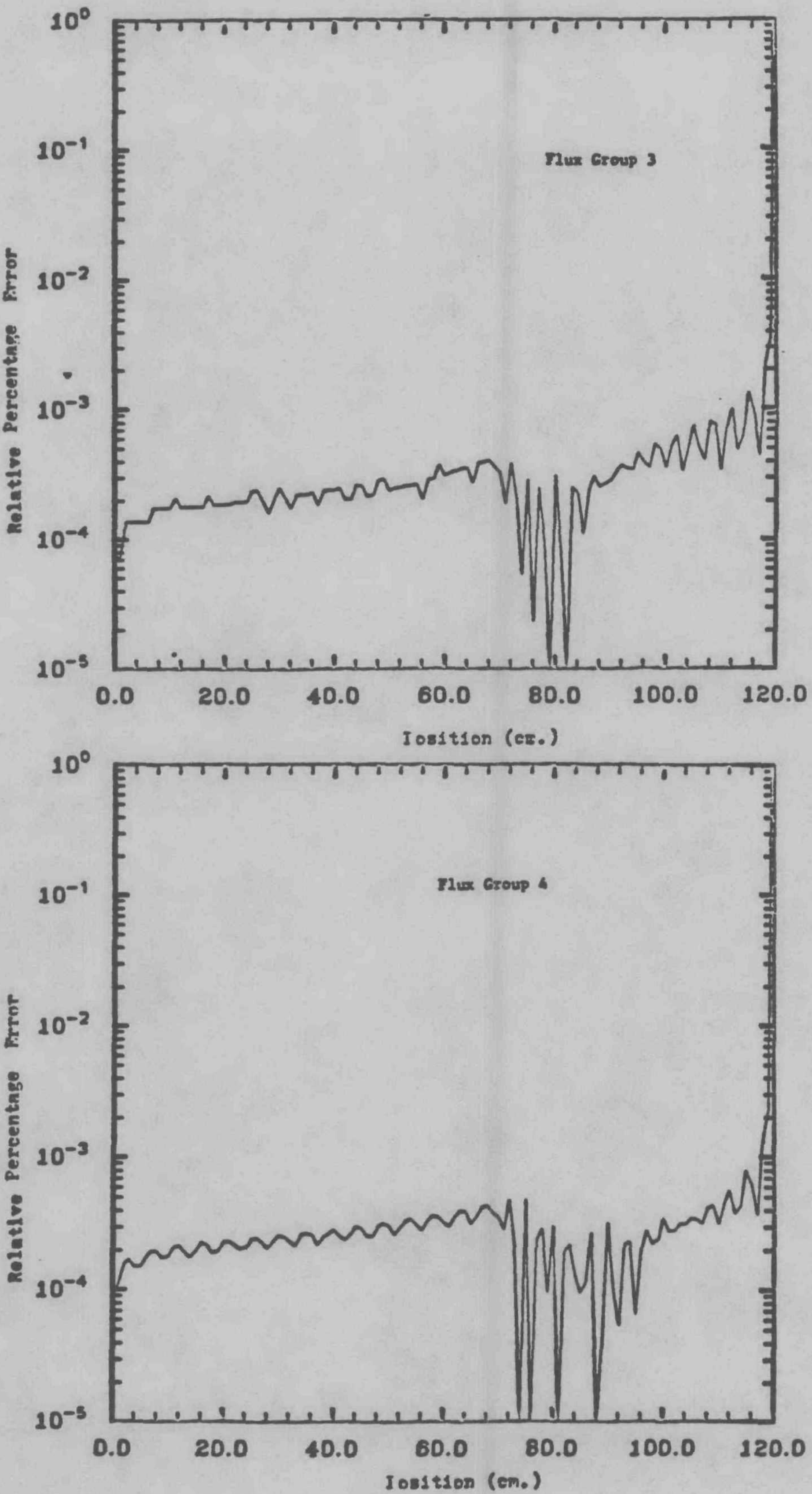

Fig. 10 Relative Percentage Error

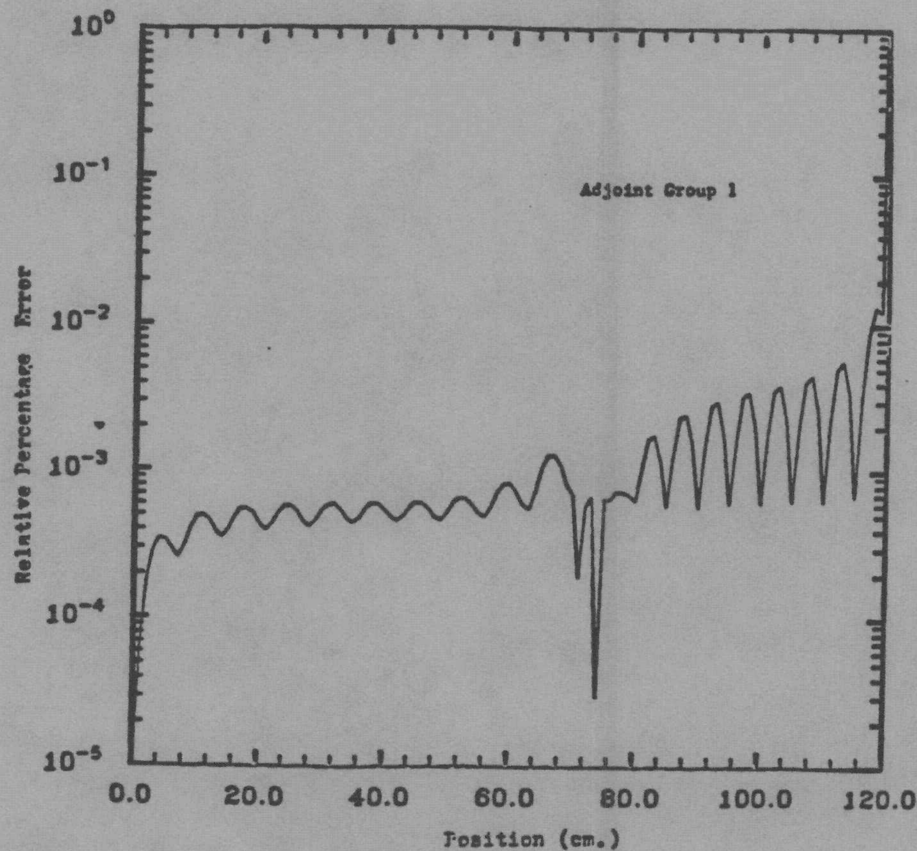

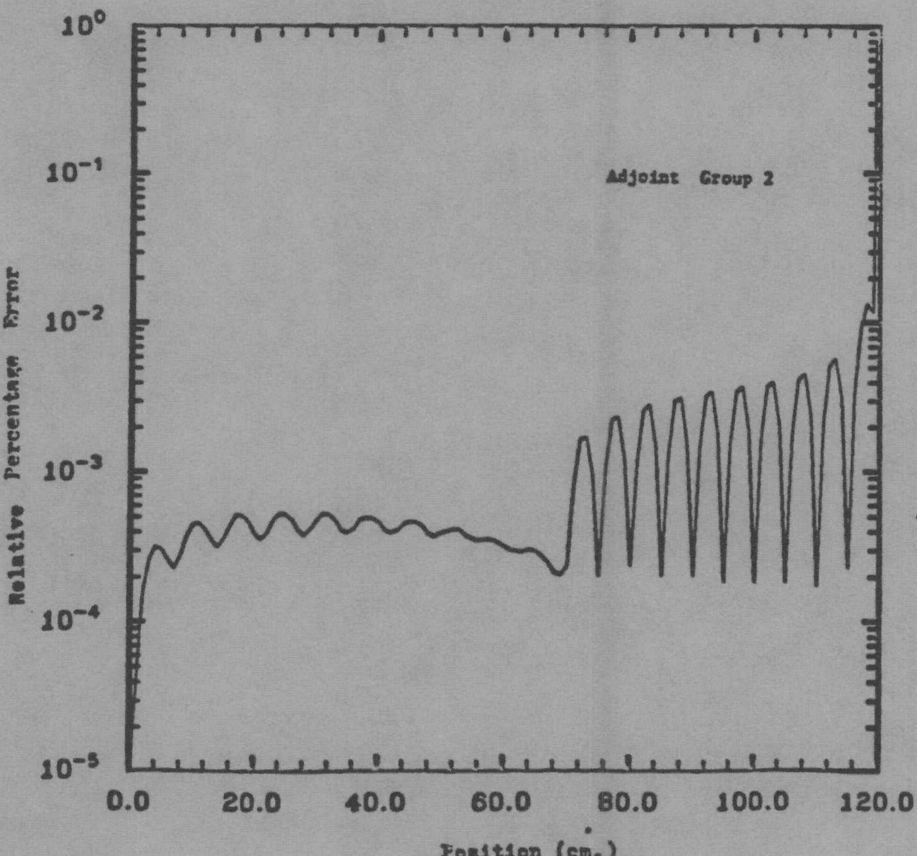

Fig. 11 Relative Percentage Error

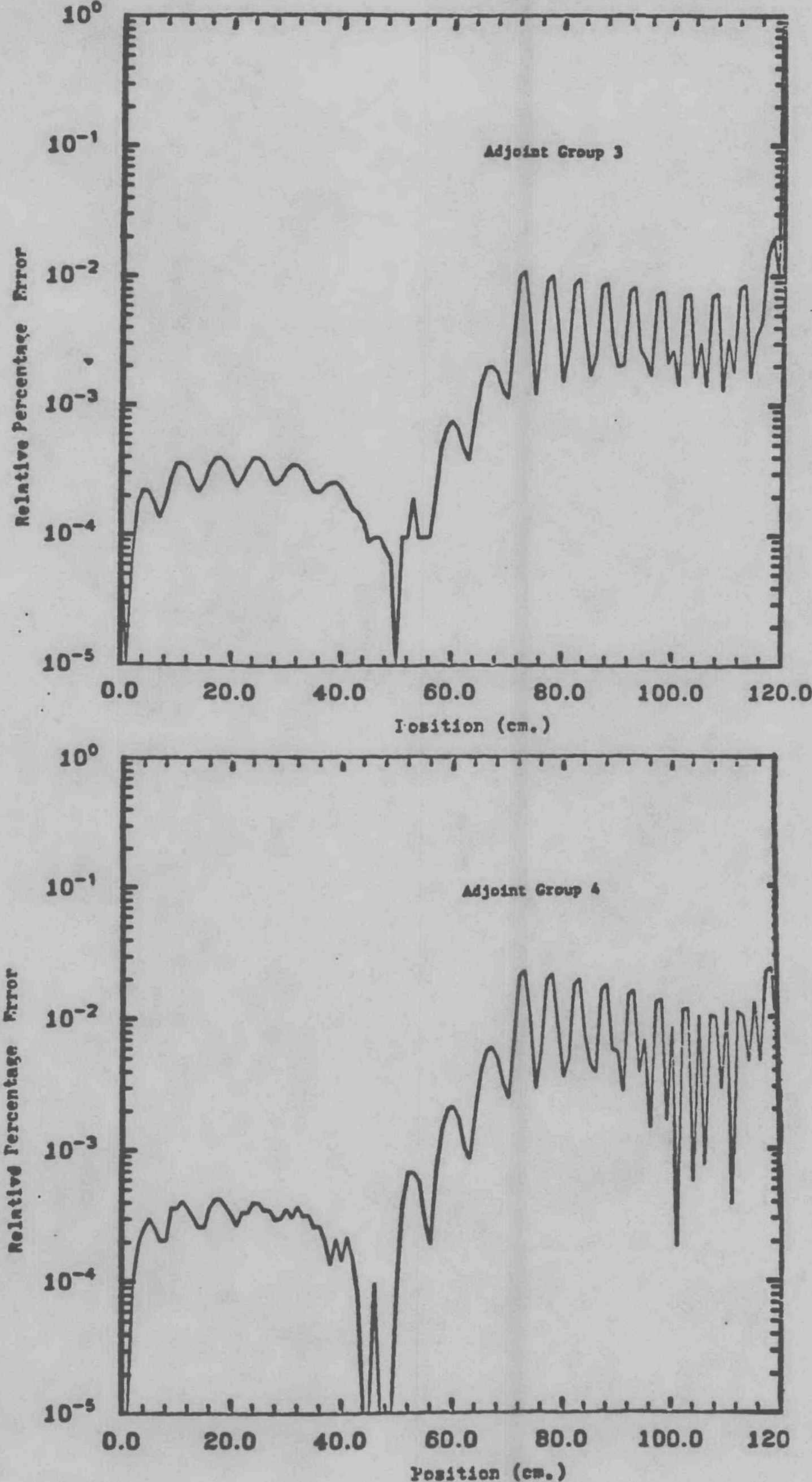

Fig. 12 Relative Percentage Error

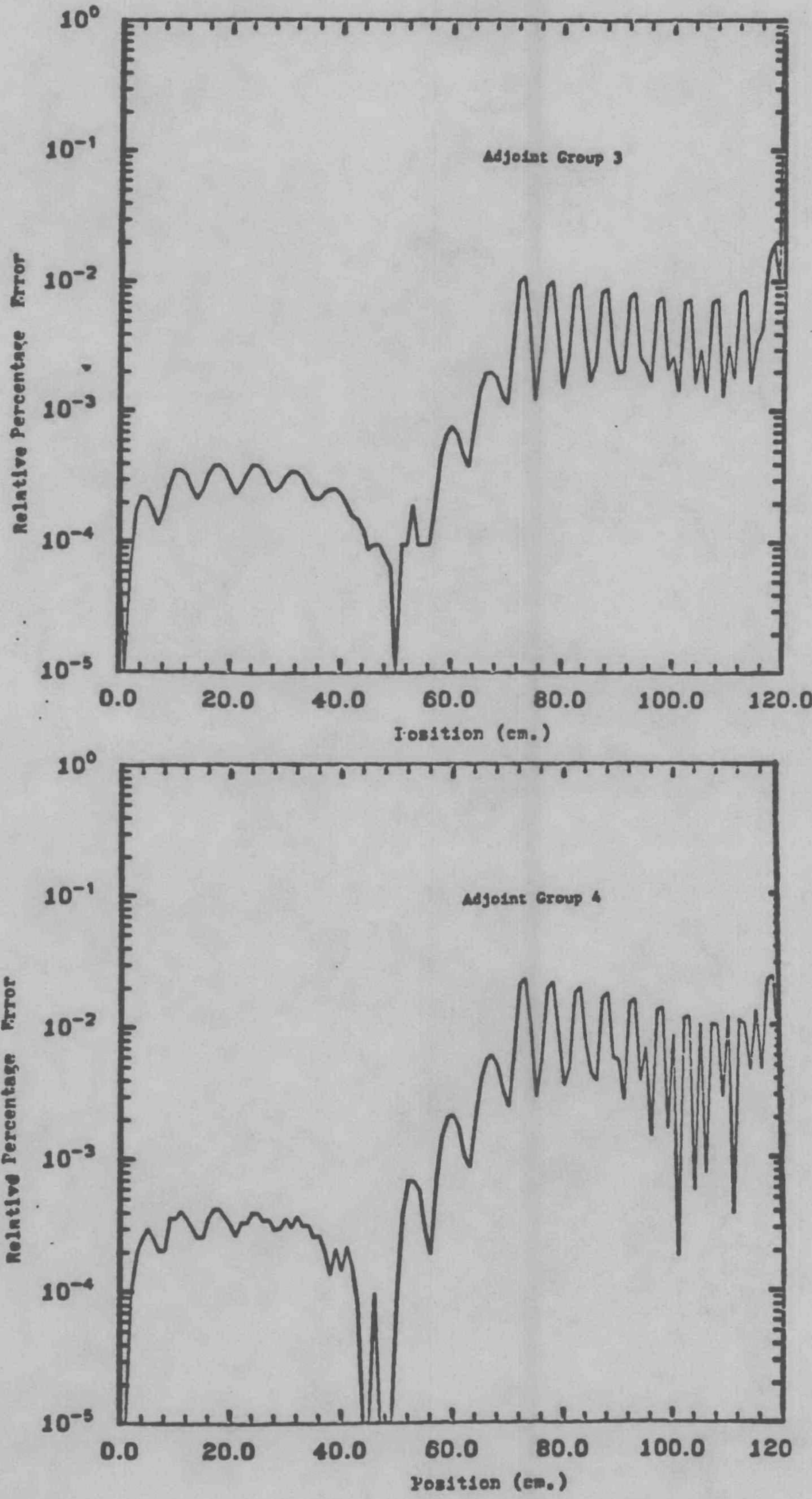

Fig. 12 Relative Percentage Error